We are IntechOpen,
the world's leading publisher of
Open Access books
Built by scientists, for scientists

4,800
Open access books available

122,000
International authors and editors

135M
Downloads

Our authors are among the

154
Countries delivered to

TOP 1%
most cited scientists

12.2%
Contributors from top 500 universities

CLARIVATE ANALYTICS
BOOK CITATION INDEX
INDEXED

WEB OF SCIENCE™

Selection of our books indexed in the Book Citation Index
in Web of Science™ Core Collection (BKCI)

Interested in publishing with us?
Contact book.department@intechopen.com

Numbers displayed above are based on latest data collected.
For more information visit www.intechopen.com

High-Quality Perovskite Film Preparations for Efficient Perovskite Solar Cells

Shangzheng Pang and Dazheng Chen

Additional information is available at the end of the chapter

Abstract

Solar cells employing organolead halide perovskite films have caught tremendous attention, and their power conversion efficiencies were stunning from 3.9% to over 22% in only 6 years. Various research reports have shown that effective controls on perovskite crystallinity, homogeneity, and surface morphology are crucial to improving the power conversion efficiencies (PCE) of perovskite solar cells. Here, based on the typical one-step and two-step deposition methods, we would like to introduce the solvent treatment mechanisms of mixed-solvent-vapor annealing and polar solvent additive, investigate the growth mode and control means of perovskite films by physical characterizations, and discuss their effects on the photovoltaic performance improvements for perovskite solar cells.

Keywords: perovskite solar cell, one-step deposition, solvent annealing, two-step deposition, solvent additive

1. Introduction

Organolead halide perovskites are emerging materials with outstanding optoelectronic properties of high absorption coefficient, broad absorption, range, adjustable band gap, solution processing, and so on [1–6]. Employing this kind of material, solar cells have caught tremendous attention, and their power conversion efficiencies (PCEs) have dramatically increased from 3.8% to over 22% in only 6 years [1, 7–9]. This great progress mainly comes from the effective controls on perovskite crystallinity, homogeneity, and surface morphology, and many researchers have focused on the first-principles modeling molecular motion and dynamic crystal structure [10, 11], defect physics [12, 13], ionic conductivity [14], hysteresis

characteristics [15], device structures and stability, and so on [16]. A high-quality perovskite film with low point defects and grain boundaries is necessary to obtain higher device PCEs.

This could greatly avoid the non-radiative recombination which could cause the loss of open-circuit voltage (V_{OC}) and decreased carrier lifetime [17–19]. On the other hand, a high-quality perovskite should also have good charge transport properties and slow ionic transport so that the free carriers could be effectively collected by the electrode and the current hysteresis behavior in current–voltage sweep measurements could be effectively avoided. In order to achieve high-quality perovskite films, a lot of deposition categories have been developed, such as one-step solution method, two-step solution method, and vapor deposition method [20–22]. And, this chapter will describe two effective solvent treatment mechanisms in typical one-step and two-step solution methods to obtain perovskite film with high-quality and relatively high PCEs.

Firstly, the early presented one-step method has still been widely used due to the advantages of low cost, simple, and more compatible with the roll-to-roll process. It is well known that the annealing treatments are crucial in one-step method to transform PbI_2-MAI-DMSO intermediate phase [23] and deposit perovskite films, and the stand-alone solvent annealing or anti-solvent annealing has been proven to be efficient for improving the perovskite quality. Here, we would like to introduce a novel solvent-engineering method, namely, the mixed-solvent-vapor annealing in the one-step solution method. Generally, the $CH_3NH_3PbI_3$ possesses a poor solubility in anhydrous isopropanol, and the annealing in this vapor environment can result in a dense uniform and pinhole-free perovskite film. When a little polar aprotic DMF or DMSO vapor is mixed with the isopropanol vapor, after the mixed-solvent-vapor annealing process, the average grain size of $CH_3NH_3PbI_3$ crystals can be further increased, thus further enhanced short-circuit current density (JSC), suppressed reverse dark current, reduced recombination loss in PSCs, and improved device stability. All devices with planar hetero-junction structure show the efficiency over 15%. What is more, by employing $CH_3NH_3I_3$-xClx perovskite precursor and interface modifying layer, the device PCE reaches around 19%.

Secondly, by incorporating a certain ratio of polar solvent such as N,N'-Dimethylformamide (DMF) into MAI/IPA precursor solution, we introduce a modified interdiffusion two-step sequential deposition method. As we all know, DMF could easily dissolve PbI_2 film while spin-coating MAI solution, and it has never been used in two-step method to fabricate perovskite film. Although DMF is a typical polar solvent for PbI_2 and perovskites, it has been found that a small ratio of DMF in the MAI solution could provide a beneficial atmosphere to promote MAI molecules diffusing into the bottom PbI_2 film and avoiding the PbI_2 residue, which is helpful to form perovskite with high quality. Simultaneously, it can also improve the surface morphology efficiently and enlarge the size of the perovskite crystal. Further, a PCE of 19.2% is achieved by the related planar heterojunction perovskite solar cells. And, this mechanism of polar solvent addition provides a facile way toward the high-quality perovskite film and high-performance devices.

As we all know, the performance of perovskite solar cells (PSCs) is strongly depending on the quality of perovskite layer. Here, based on the typical one-step and two-step deposition methods, we would like to introduce the solvent treatment mechanisms of mixed-solvent-vapor annealing and polar solvent additive to investigate the growth mode and control the means of perovskite films by physical characterizations and discuss their effects on the photovoltaic performance improvements for perovskite solar cells.

2. One-step method: prepared perovskite film

2.1. Film formation

The $CH_3NH_3PbI_3$ precursor solution was prepared by mixing 1.4 M PbI_2 and 1.35 M MAI dissolved in the co-solvent of DMSO:GBL (3:7 v/v) and stirred for 2 h at 70°C. The $CH_3NH_3I_3$-xClx precursor solution was prepared by mixing 1.26 M PbI_2, 0.14 M $PbCl_2$, and 1.35 M MAI was dissolved in the co-solvent of DMSO:GBL (3:7 v/v), and was stirred for 2 h at 70°C. The solution was then spin-coated onto the PEDOT:PSS layer with solvent-engineering method. Briefly, the spin-coating process was programmed to run at 1000 rpm for 15 s and then 5000 rpm for 25 s. When the spinning was at 37 s, 350 μl anhydrous toluene was injected onto the substrates. The perovskite films were solvent or thermally annealed on the hot plate at 100°C for 20 min. For the film treated with solvent annealing, the perovskite films were put on top of a hot plate and covered by a glass Petri dish. Around 40 μl of IPA, IPA:DMF (100:1 v/v) or IPA:DMSO (100:1 v/v) solvent was added around the substrates during the thermal anneal-ing process, so that the solvent vapor could make contact with the perovskite films. More experimental details can be found in our previous work [24].

2.2. Results and discussion

The $CH_3NH_3PbI_3$ film morphologies and surface textures are investigated by atomic force microscopy (AFM) and scanning electron microscopy (SEM). As is shown in **Figure 1**, the root-mean-square (RMS) roughness value of the pristine $CH_3NH_3PbI_3$ film is 8.28 nm; this result is consistent with the report [23] by using the solvent-engineering method. Introducing the IPA vapor in the annealing process, the minimum RMS value of the $CH_3NH_3PbI_3$ film is achieved. The introduced liquid anhydrous isopropanol on the hot plate turns to gas rapidly in a confined space which produces a certain anti-solvent vapor pressure and retards the crystal formation of perovskite to improve the crystalline quality [25, 26]. When the polar aprotic sol-vents of DMSO and DMF are introduced in the IPA vapor annealing process, the RMS values increase to 10.51 and 9.04 nm, respectively. As we all know, $CH_3NH_3PbI_3$ is easily dissolved in DMSO and DMF, and a trace of DMSO or DMF introduced in the annealing process can induce a recrystallization process of $CH_3NH_3PbI_3$ leading to the change of the morphology and surface. The film quality can improve by precise control of the recrystallization process. However, an excessive polar aprotic solvent vapor will produce a negative effect and reduce the film quality. As discussed above, the DMSO vapor will be released by the PbI_2-MAI-DMSO intermediate phases. With extra DMSO introduced in the annealing process, the DMSO vapor will be excessive. This causes the largest RMS value in the perovskite film, which may be one of the reasons for the lower device performance than the IPA PSCs. Therefore, the introduced DMF is more suitable than DMSO, and the corresponding devices show a better performance.

It is shown in the SEM image (**Figure 2a**) that the pristine $CH_3NH_3PbI_3$ film has a small grain size in the range of 100–300 nm. Bright portions at the grain boundaries can be observed, which is likely to be less conductive PbI_2 as in the previous reports [23]. In addition, there are also spots of pinholes on the film surface. The charge transport and the photovoltaic perfor-mance [26] are strongly influenced by these defects. The average grain size of the $CH_3NH_3PbI_3$
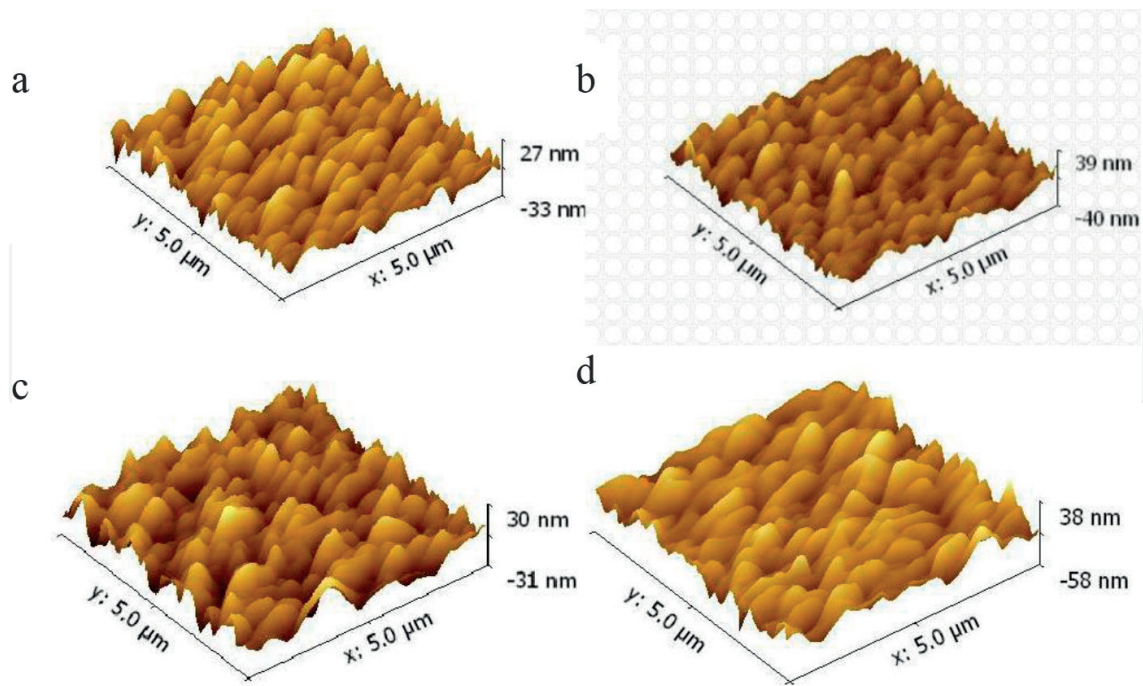
Figure 1. AFM images of perovskite films via (a) pristine, (b) IPA, (c) IPA/DMSO, and (d) IPA/DMF vapor annealing. The measured RMS values are (a) 8.28 nm, (b) 7.87 nm, (c) 10.51 nm, and (d) 9.04 nm (reprinted with the permission from [24], 2016, Elsevier).
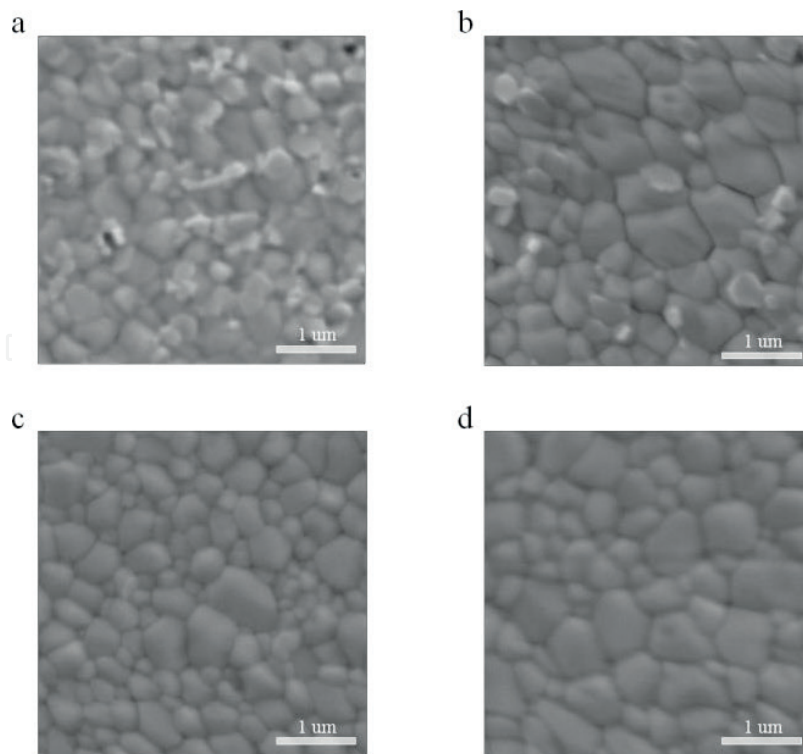

Figure 2. SEM images of perovskite films via (a) pristine, (b) IPA, (c) IPA/DMSO, and (d) IPA/DMF vapor annealing (reprinted with permission from [24], 2016, Elsevier).

has been increased with the obvious reduction of pinholes (**Figure 2b**) after treating the anhydrous IPA vapor in the annealing process. Then, the $CH_3NH_3PbI_3$ films become more compact and dense, and the pinholes disappear as shown in **Figure 2c** and **d** when the polar aprotic solvent of DMSO or DMF is further introduced in the annealing process. However, there is an obvious difference between the IPA/DMSO and IPA/DMF that resulted in perovskite films. The grain size of the IPA/DMF $CH_3NH_3PbI_3$ film is obviously larger than that of the IPA/DMSO $CH_3NH_3PbI_3$ film. The boundary defects and related recombination are reduced for the high crystalline, large grain size, and a small grain boundary area. This will benefit the charge transport and charge collection, which could be another reason for the better performance of IPA/DMF devices.

Figure 3 shows the XRD patterns of pristine, IPA, and IPA/DMF $CH_3NH_3PbI_3$ films. The formation of $CH_3NH_3PbI_3$ is proven by the diffraction peaks around 14.21, 28.51, and 31.88°, which are assigned to the (110), (220), and (310) lattice planes of the tetragonal perovskite structure, respectively. And, the improved crystallinity of the perovskite films annealed in IPA and IPA/DMF vapor has been confirmed by the stronger and sharper XRD diffraction peaks than that of pristine $CH_3NH_3PbI_3$. Significantly, the solvent annealing reduces the small peak at 12.8° belonging to PbI_2, which is in line with the previous SEM results. The $CH_3NH_3PbI_3$ film treated by the mixed IPA/DMF vapor shows stronger and sharper peaks, which reveals the higher crystallization. This again explains why the IPA-/DMF-treated devices acquire the best performance.

To fabricate perovskite solar cells, there are two typical device structures of mesoporous and conventional planar structure. Mesoporous device structures employing an n-type TiO_2
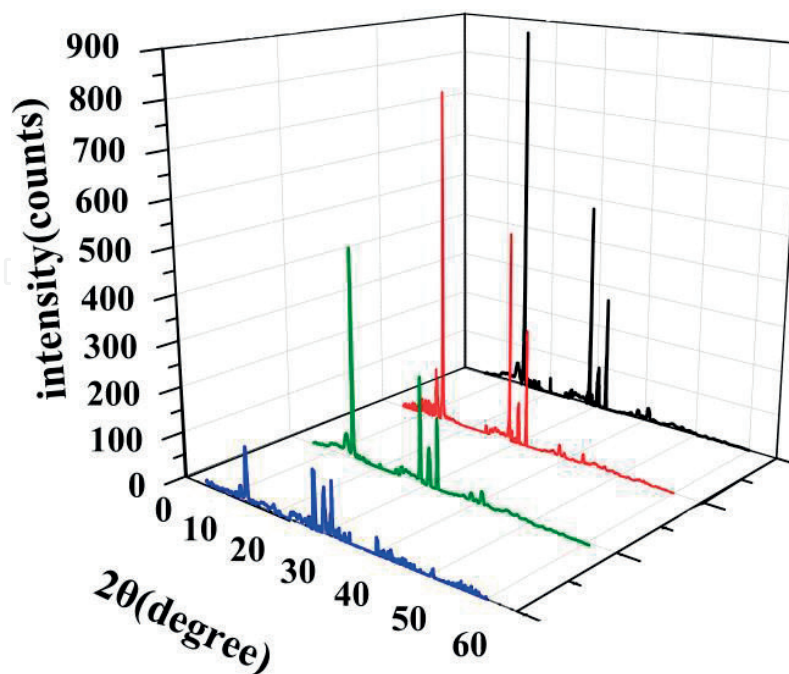

Figure 3. XRD patterns of CH3NH3PbI3 films with pristine (blue), IPA/DMSO vapor (green), IPA vapor (red), and IPA/DMF vapor (black) annealing (reprinted with the permission from [24], 2016, Elsevier).

layer as the bottom electron transport layer. A high-temperature (>450°C) sintering process for the TiO$_2$ scaffold, which is a great limitation on the substrate and increases the cost, is required. On the other hand, the conventional planar structures based on TiO$_2$ usually suffer from a large degree of J–V hysteresis. In 2013, Guo developed the first planar heterojunction perovskite solar cell with inverted structure design. The p-type layer was deposited before the perovskite film, while the n-type layer was deposited after the perovskite film [27]. This architecture was defined as p-i-n structure or inverted structure. Recent studies have shown that the inverted planar PSCs adopted in this study show negligible J–V hysteresis and promising device performance [28, 29]. Thus, the PSCs in this work adopt the inverted structure of ITO/PEDOT:PSS/CH$_3$NH$_3$PbI$_3$/PCBM/Ag (shown in **Figure 4(a)**), where the PCBM and PEDOT:PSS act as electron and hole transport layers, respectively.

The corresponding energy band diagram is illustrated in **Figure 4(b)**. PEDOT:PSS has the conduction band energy of around −3.0 eV and the valance band of around −5.2 eV, which suggests that holes from CH$_3$NH$_3$PbI$_3$ can be transported to PEDOT:PSS and collected by the anode, while electrons from CH$_3$NH$_3$PbI$_3$ can be blocked. In other words, this PEDOT:PSS acts as an electron-blocking layer and a hole extraction layer. At the same time, the PCBM layer plays the role of electron extraction layer, and it can effectively aid the electron transport to the cathode. Furthermore, it has been reported that PCBM can effectively passivate CH$_3$NH$_3$PbI$_3$ and minimize the J–V hysteresis [30]. This structure is expected to obtain better photovoltaic performance for perovskite solar cells.

The J–V characteristics of the fabricated CH$_3$NH$_3$PbI$_3$ PSCs are shown in **Figure 5(a)**, and their photovoltaic parameters are summarized in **Table 1**. The "pristine" represents the PSCs without the vapor treatment in the perovskite annealing process. The "IPA," "IPA/DMF (100:1 v/v)," and "IPA/DMSO (100:1 v/v)" represent the PSCs treated by corresponding vapors. It can be seen that the pristine PSCs exhibit an average PCE of 11.5%, with JSC = 17.1 ± 0.7 mA/cm^2, VOC = 0.96 ± 0.02 V, and FF = 70.1 ± 1.6%, and the best one shows a PCE of 12.2% with JSC = 18.1 mA/cm^2, VOC = 0.96 V, and FF = 70.1%. It is obvious that the PCE is mainly limited by the relatively low JSC, which is in line with the relatively low PCE for inverted planar PSCs [23]. However, by introducing the solvent vapor in the annealing process, the resulted PSCs show a significant improvement in
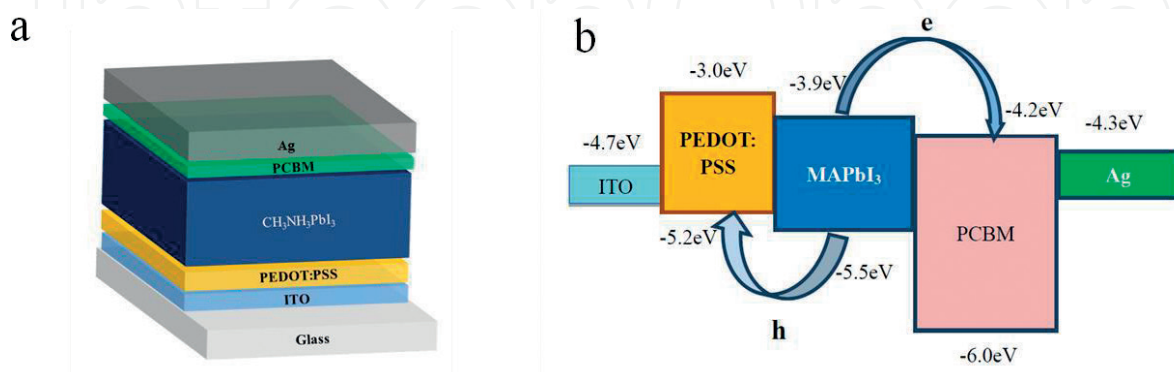

Figure 4. (a) Schematic structure of the devices in this study: ITO/PEDOT:PSS/CH$_3$NH$_3$PbI$_3$/PCBM/Ag. The thickness of each layer was not in scale with the real thickness for clarity. (b) Schematic illustration of energy band diagram of studied devices (reprinted with the permission from [24], 2016, Elsevier).
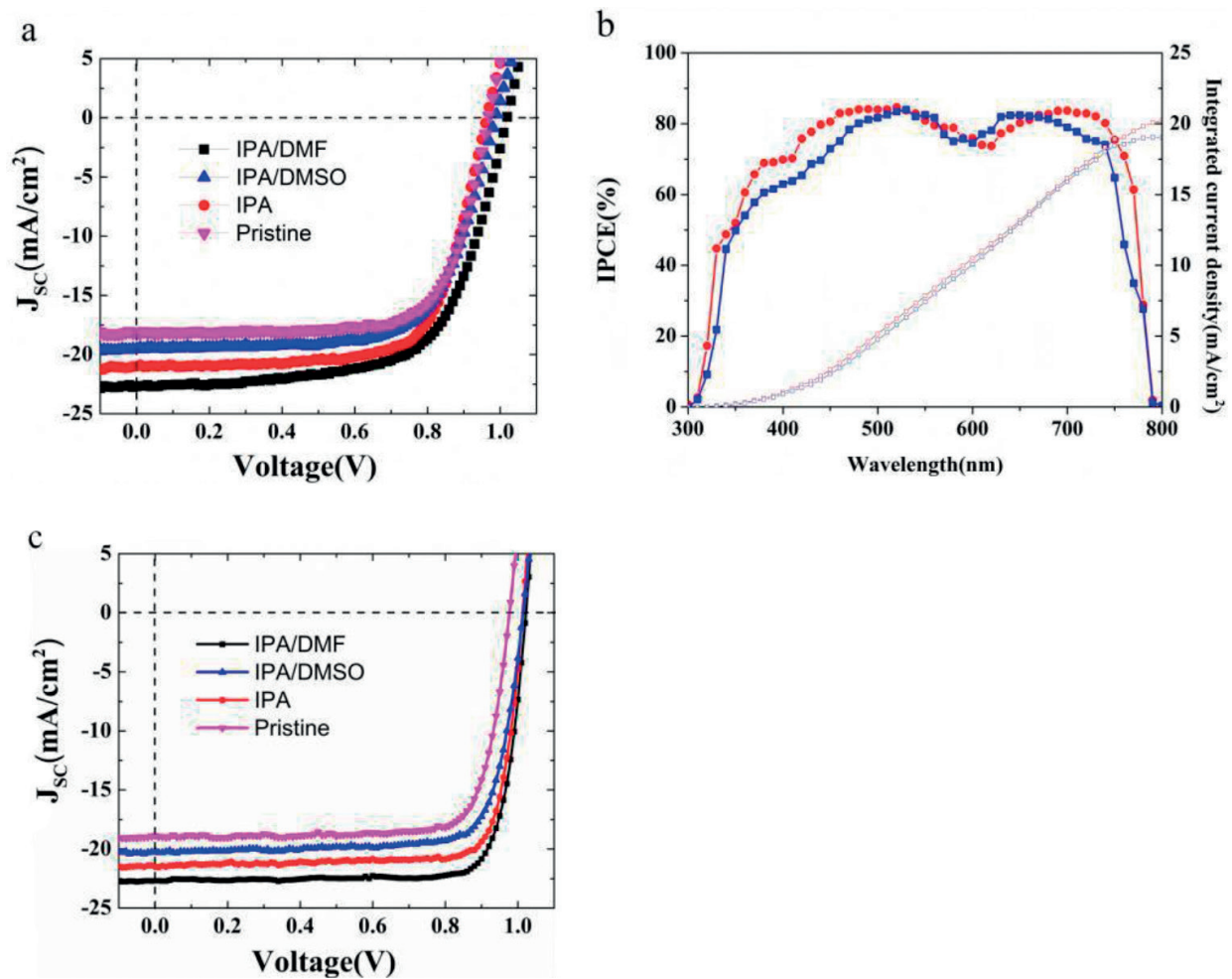
Figure 5. (a) *J–V* characteristics of $CH_3NH_3PbI_3$ PSCs without solvent annealing and with IPA, IPA/DMSO, or IPA/DMF solvent annealing under the simulated AM 1.5G illumination of 100 mW/cm². (b) IPCE curves and integrated current density of IPA PSCs (blue) and IPA/DMF PSCs (red). (c) *J–V* characteristics of $CH_3NH_3I_3$–xClx PSCs without solvent annealing and with IPA, IPA/DMSO, or IPA/DMF solvent annealing under the simulated AM 1.5G illumination of 100 mW/cm² (reprinted with the permission from [24], 2016, Elsevier).

performance (see **Figure 5b**). For the IPA PSCs, the greatly improved *J*SC of 19.8 ± 0.5 mA/cm² is obtained, as well as a slightly increased FF (70.4 ± 1.2) and *V*OC (0.98 ± 0.01 V); thus, the average PCE increased to 13.2% and the highest PCE of 14.2%(*J*SC = 20.9 mA/cm²). It is suggested that the IPA vapor treatment can help enhance the $CH_3NH_3PbI_3$ crystallinity during the annealing process and thus improve the photovoltaic performance of PSCs. When the DMSO vapor is further introduced, the IPA/DMSO PSCs show an average PCE of 12.3% with *J*SC = 19.0 ± 0.7 mA/cm², *V*OC = 0.99 ± 0.01 V, and FF = 65.7 ± 1.8%, which is relatively inferior to the IPA PSCs. This is related to the PbI_2-MAI-DMSO intermediate phases and can be understood from the annealing process. Since the perovskite formation is reversible, the transform of PbI_2-MAI-DMSO intermediate phases will release extra DMSO vapor, combining with the introduced DMSO, and the excessive DMSO vapor would further affect the recrystallization of $CH_3NH_3PbI_3$ by shifting the reaction along the decomposition direction. However, when the IPA-/DMF-mixed vapor is adopted in the annealing process, the corresponding PSCs show an obviously improved *J*SC of 20.8 ± 0.6 mA/cm², *V*OC of 1.02 ± 0.01 V, and FF of 67.0 ± 1.5% and the PCE average values of 14.2%, and the

CH3NH3PbI3 PSCs	VOC (V)	JSC mA/cm^2	FF (%)	PCE (%)
Pristine	0.96 ± 0.02	17.14 ± 0.71	70.1 ± 1.6	11.5(12.2)
IPA	0.98 ± 0.01	19.85 ± 0.54	70.4 ± 1.2	13.2(14.7)
IPA/DMSO	0.99 ± 0.01	19.03 ± 0.73	65.7 ± 1.8	12.3(13.1)
IPA/DMF	1.02 ± 0.01	20.81 ± 0.56	67.0 ± 1.5	14.2(15.1)
CH3NH3I3-xClx PSCs	VOC (V)	JSC mA/cm^2	FF (%)	PCE (%)
Pristine	0.98 ± 0.01	19.00 ± 0.82	79.2 ± 0.6	14.0(14.3)
IPA	1.00 ± 0.01	20.83 ± 0.77	81.5 ± 0.5	17.3(18.1)
IPA/DMSO	1.00 ± 0.01	20.30 ± 0.58	78.0 ± 1.5	15.9(16.3)
IPA/DMF	1.02 ± 0.01	22.23 ± 0.50	80.6 ± 1.3	18.0(18.9)

The average results were based on ten devices.

Table 1. Photovoltaic parameters of $CH_3NH_3PbI_3$ and $CH_3NH_3I_3$-xClx PSCs under simulated AM 1.5G illumination (100 mW/cm^2) (reprinted with the permission from [24], 2016, Elsevier).

best one obtains a PCE of 15.1% and a JSC of 22.7 mA/cm^2. Compared with the PSCs with alone IPA vapor, it is clear that both JSC and VOC are strikingly enhanced for PSCs treated with IPA-/DMF-mixed vapor. In this work, the optimized ratio of IPA/DMF is 100:1(v/v), while the excessive DMF will be also destructive to the perovskite formations [24]. Additionally, the incident photo-to-electron conversion efficiency (IPCE) curves and the integrated current density are shown in **Figure 5b**. It is clear that the PSC treated with IPA-/DMF-mixed vapor shows a higher IPCE value at most wavelengths, as well as the largely integrated current density of 20.3 mA/cm^2, which is very close to the measured JSC in J–V characteristic.

To further improve the photovoltaic performance of inverted PSCs, the $CH_3NH_3I_3$-xClx precursor and BCP interface layer have been employed, and the resulted PSCs show a structure of $ITO/PEDOT:PSS/CH_3NH_3I_3$-xClx/PCBM/BCP/Ag. The measured photovoltaic parameters are summarized in **Table 1**. Without solvent annealing treatment, the pristine $CH_3NH_3I_3$-xClx device exhibits a relatively poor performance with JSC = 19.0 ± 0.82 mA/cm^2, VOC = 0.98 ± 0.01 V, and FF = 79.2 ± 0.6% and an average PCE of 14.0%. With anti-solvent vapor treatment in the annealing process, the performance of $CH_3NH_3I_3$-xClx device has been significantly improved compared with the pristine devices. For the IPA $CH_3NH_3I_3$-xClx PSCs, the JSC is greatly improved to 20.83 ± 0.77 mA/cm^2 with nearly unchanged VOC and FF. Thus, the average PCE of 17.3% and the highest PCE of 18.1% are achieved. Compared to the IPA $CH_3NH_3I_3$-xClx device, IPA/DMF $CH_3NH_3I_3$-xClx device shows a higher average PCE of 18.0% (the best device shows PCE of 18.9%) with VOC = 1.02 ± 0.01 V, JSC = 22.23 ± 0.50 mA/cm^2, and FF = 80.6 ± 1.3%.

Besides the efficiency of PSCs, the stability is another critical limitation for their commercial applications. The structural chemical stability of perovskite could be damaged by many factors such as interaction with moisture and oxygen especially at high temperatures. For the ITO/PEDOT:PSS/perovskite/PCBM/Ag structure, the hydrophilic and acidic nature of PEDOT:PSS is considered an unstable transport layer, also the possible oxidation of silver electrode. Here, we mainly discuss the device stability issue related to the perovskite layers. As we know, the stability of perovskite is related to its material nature [21], and also the preparation process and treatment have direct effects on the crystalline quality. For the un-encapsulated PSCs processed at different annealing conditions, we tested them in an ambient environment at 22°C with about 30% humidity. The degradation of key photovoltaic parameters of PCE, JSC, VOC, and FF are shown in **Figure 6**. After 8 days in air, the PCE of the pristine PSC kept 40% of the initial efficiency, with FF and JSC reduced to 59 and 70% of the original values. It should be noted that the device stability was significantly improved for the PSCs treated by IPA vapor and IPA/DMF mixed solvent vapor. And, the PCEs could keep 65 and 74% of the initial values after 8 days. This indicates the relationship of perovskite quality and device stability and provides a strategy to obtain high-efficient PSCs with good stability.
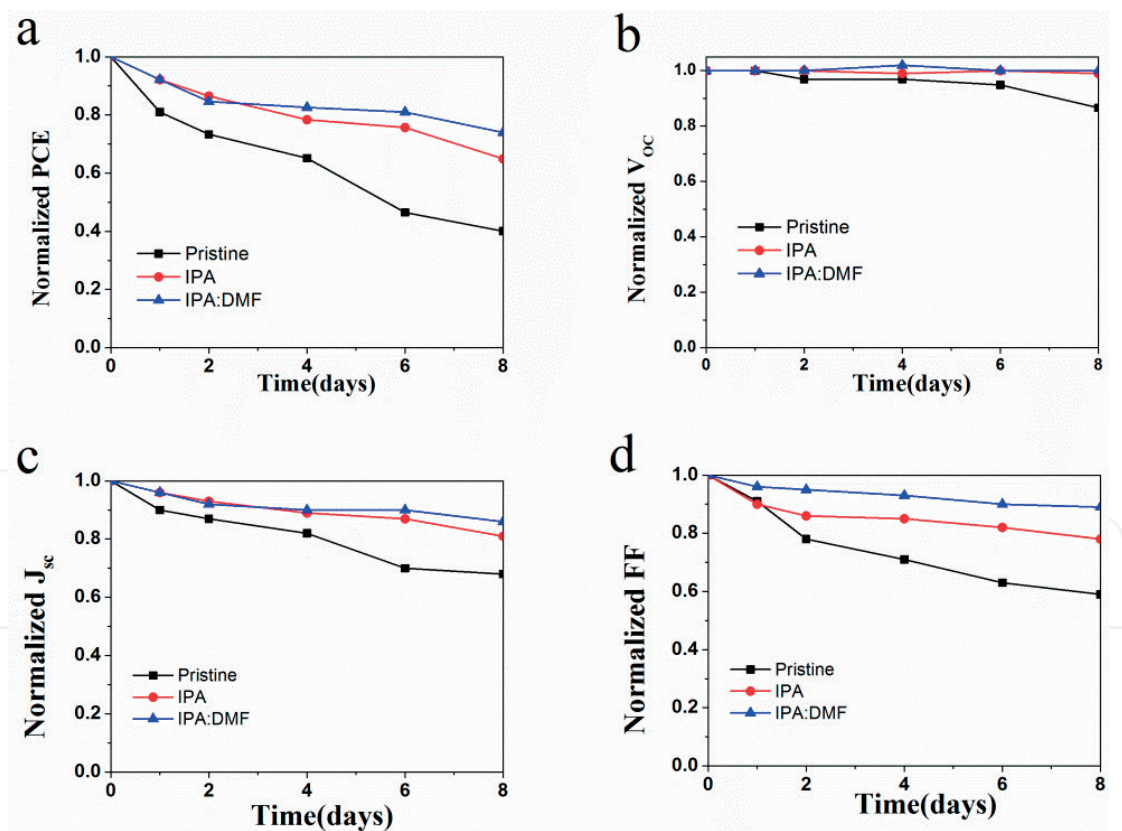

Figure 6. Stability of the devices with the structure of ITO/PEDOT:PSS/perovskite/PCBM/Ag: (a) normalized PCE, (b) normalized VOC, (c) normalized JSC, and (d) normalized FF (reprinted with the permission from [24], 2016, Elsevier).

3. Two-step method: Prepared perovskite film

3.1. Film formation

0.85 M PbI_2 and 0.15 M $PbCl_2$ were dissolved in the solvent of DMF and stirred for 2 h at 75°C. Forty milligrams of MAI were dissolved in the solvent of IPA with/without additionally 0.9 vol% DMF or GBL, respectively. Around 60ul PbX_2 precursor solution preheated to 75°C was transferred by pipettes to the ITO substrates. Briefly, the spin-coating process was programmed to run at 3000 rpm for 45 s, and a yellow transparent dense PbI_2 film was deposited. Then, MAI was spin-coated on top of the dried PbI_2 layer at room temperature at 3000 rpm for 45 s. All of the films were thermally annealed on the hot plate at 100°C for 10 min. And, the perovskite film is formed by interdiffusion process. **Figure 7** shows the photographs of perovskite films deposited by MAI/IPA and MAI/(IPA-0.9%DMF) solutions. It can be seen that the perovskite film shows a heterogeneous and whitish surface morphology if the pure MAI/IPA solution was used. And, the concentration variation of the MAI/IPA solution cannot reverse the situation. However, by introducing proper DMF (0.9%) solvent additive into the MAI/IPA solution, the dark brown perovskite film is obtained, and the optimized MAI concentration is 40 mg/L. To further know their difference, the morphology and crystalline quality of perovskite films were measured by scanning electron microscopy (SEM) and X-ray diffraction (XRD) tests, as well as their optical property by UV–visible spectrophotometer and photoluminescence spectra. More experimental details can be found in our previous work [36].

3.2. Results and discussion

Figure 8(a) and **(b)** displays the scanning electron microscopy (SEM) images of perovskite films. The perovskite film without DMF additive shows the small grain size and many pinholes between the grain boundaries (marked with the red circles). These defects increase recombination probability and severely hamper the charge transport and the device performance. However, when a small amount of DMF is added to MAI/IPA precursor, those pinholes among the grain boundaries are effectively eliminated in the resulted perovskite films, as shown in **Figure 8(b)**; also, the average grain size of perovskite is obviously increased.
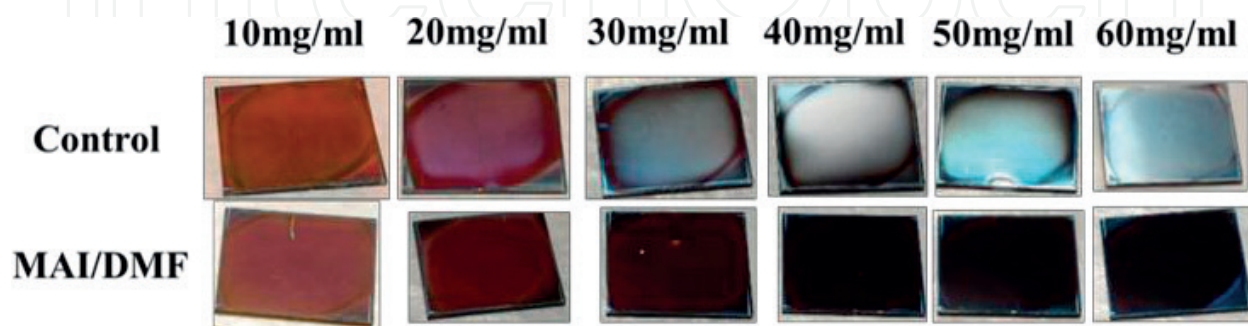

Figure 7. Photographs of perovskite films by spin-coating MAI/IPA solution (top) and MAI/(IPA-0.9%DMF) (bottom), respectively, with 10, 20, 30, 40, 50, and 60 mg/ml MAI concentrations (from left to right) (reprinted with the permission from [31], 2017, The Royal Society of Chemistry).
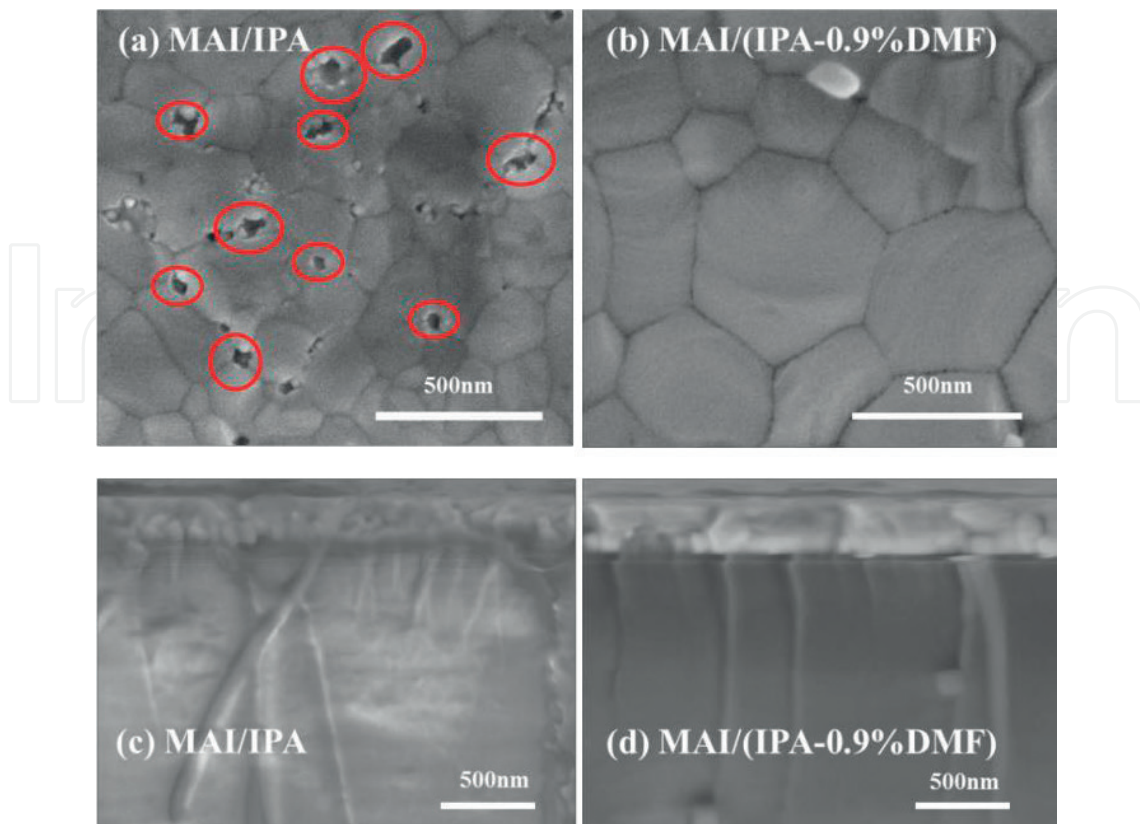
Figure 8. SEM images of perovskite films. Higher-magnification SEM image of the perovskite film without (a) and with (b) DMF additive, cross-sectional SEM image of the perovskite film without DMF additive (c) and with (d) DMF additive (reprinted with the permission from [31], 2017, the Royal Society of Chemistry).

Figure 8(c) and **(d)** displays the cross-sectional images of perovskite films deposited on glass substrate. While using MAI/IPA solution, the perovskite film shows the low-quality, incomplete-reaction PbI_2 and small grain size. However, by adding proper DMF into MAI precursor solution, a perovskite film with large grain size could be observed from **Figure 8(d)**. **Figure 9** shows the forming process of perovskite film by two-step deposition method. It is obvious that the controlled perovskite film seemed a bit low quality with the little crystal and more defects when the bare MAI/IPA solution were used. However, with proper DMF solvent additive doped into the MAI/IPA solution, the crystal quality of perovskite film could significantly be improved.

According to the high solubility of MAI and PbI_2 in DMF, we present a possible mechanism that [31] the small amount of DMF solvent provides a "wet" environment so that PbI_2 and MAI could react with each other and later a high-quality perovskite could be obtained after annealing. As we know, the DMF has a higher boiling point (152.8°C) that of IPA; thus, the presence time of DMF is relatively long during the 100°C annealing process. During the crystal growth process, the DMF additive could drive the MAI penetrating into the thick PbI_2 to form larger crystal grains by slowing down the perovskite crystallization rate, and a thick film with a pure phase since perovskite can be totally but very slowly dissolved in DMF, and the dissolving process depends on the amount of DMF. Moreover, proper DMF solvent vapor annealing could increase thin-film crystallinity, and crystalline domain size since the
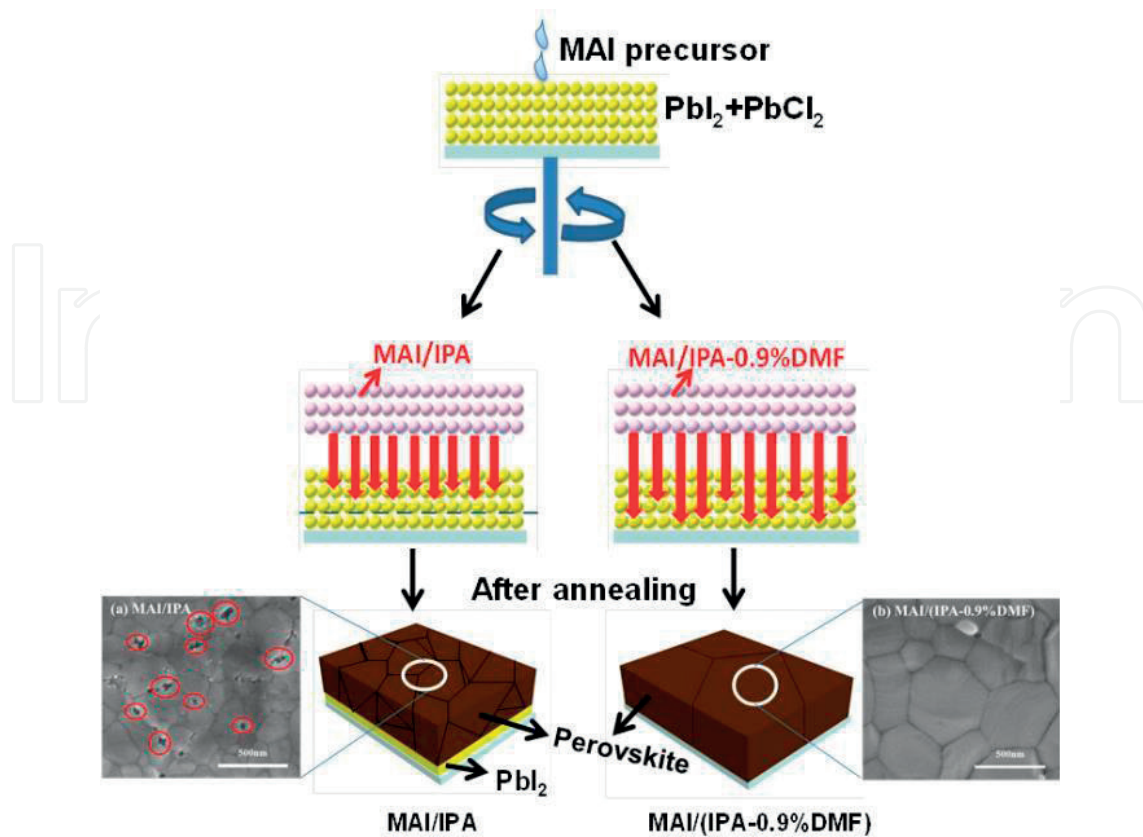
Figure 9. The schematic of interdiffusion procedure for preparing the uniform and dense perovskite film (reprinted with the permission from [31], 2017, the Royal Society of Chemistry).

DMF solvent could induce a second perovskite dissolution and recrystallization process. As a result, the large-size crystal grains and high-quality perovskite films are achieved, which can be partly supported by the SEM images. To verify this mechanism, the crystal quality, light absorption ability, and charge transport property are discussed as follows.

Figure 10(a) shows the XRD results of PbI_2, MAI, and perovskite films. As expected, the PbI_2 displays a characteristic diffraction peak at 2θ of 12.8°. And, the diffraction peaks of MAI at 2θ of 9.8, 19.65, and 29.65° are consistent with reported results. For the perovskite film without DMF additive, the diffraction peak at 12.8° means the PbI_2 residues in this film. However, when a 0.9 vol% DMF is added to MAI/IPA precursor, the PbI_2 diffraction peak disappears, and the peak intensity of perovskite is enhanced; both of them demonstrate the higher crystal quality of perovskite film. It is suggested that the presence of a small amount of DMF solvent could improve the complete conversion of PbI_2 to perovskite by promoting the reaction between PbI_2 and MAI. **Figure 10(b)** displays the steady-state PL spectra of the perovskite films on the glass or glass/ITO/PEDOT:PSS substrates. For the perovskite films on glass, the same peak position at 759 nm is observed; the PL peak intensity is enhanced after adding the DMF additive in MAI precursor, which demonstrates the improved perovskite film quality. Furthermore, for the perovskite/PEDOT:PSS/ITO/glass sample, the more obvious PL quenching in perovskite with DMF additive means the more efficient charge transfer from the perovskite to the PEDOT:PSS layer, which agrees the XRD discussion of the complete conversion of PbI_2 to perovskite. While
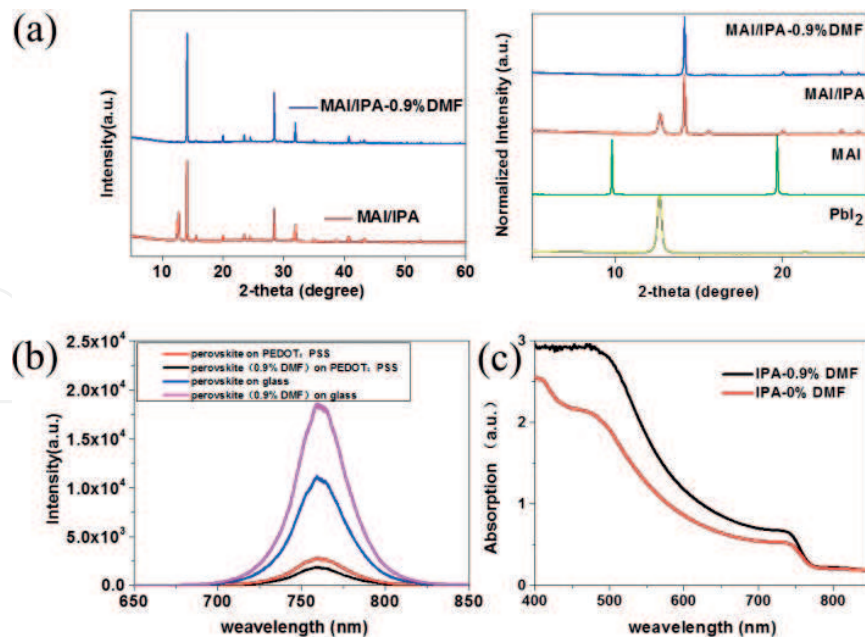
Figure 10. (a) XRD spectra of perovskite with MAI/IPA and MAI/IPA-0.9% DMF, respectively. (b) Normalized intensity of X-ray diffraction spectra of perovskite, PbI$_2$ and MAI, respectively. (c) Photoluminescence (PL) spectra at room temperature. Perovskite films grown on different substrates including glass or PEDOT:PSS. (d) Absorption spectra of the perovskite films, which were fabricated by spin-coating MAI/IPA and MAI/IPA-0.9%DMF on dried PbI$_2$ films (Reprinted with the permission from [31], 2017, the Royal Society of Chemistry).

for the perovskite without DMF additive, the low quenching efficiency can be attributed to the charge block effect of residual PbI$_2$ at perovskite/PEDOT:PSS interface. **Figure 10(c)** displays the absorption spectra of the perovskite films. It is clear that the light absorption in the perovskite film with 0.9% DMF additive is more efficient than the perovskite film without DMF additive at all absorption wavelength range. **Figure 11** exhibits the device structure of the perovskite solar cell and the corresponding energy diagram. In the device the highest occupied molecular orbital (HOMO) level and the lowest unoccupied molecular orbital (LUMO) level of PEDOT:PSS are 3.0 and 5.2 eV, respectively. So, the PEDOT:PSS layer plays the role of electron-blocking layer and hole transport layer. Correspondingly, the PCBM acts as hole-blocking layer and electron transport layer with the HOMO level of 4.0 eV and LUMO level of 6.2 eV. The BCP is used as the interface modification layer with the HOMO level of 7.0 eV. The Ag film and the ITO are chosen as the top and bottom electrodes.

Based on the high some batches of devices were fabricated, and **Figure 12(a)** displays typical *J*–*V* characteristics of the fabricated PSCs. Without DMF additive, the PSC exhibits a short- circuit current density (*J*SC) of 16.16 mA/cm^2, an open-circuit voltage (*V*OC) of 0.99 V, and a fill factor (*FF*) of 71.2% and a corresponding PCE of 11.4%. It is obvious that the low *J*SC and *FF* are the main factors limiting the PCE. Compared with the PSC without DMF additive, the PSC performance has been greatly improved as shown in **Figure 12(a)**, when the DMF is first introduced in the MAI solution. Consequently, *J*SC is greatly improved to 20.06 mA/cm^2, and *FF* is improved to 77.1% with a slightly increased *V*OC (1.00 V), which enhances the PCE to 15.5%. It can be inferred that the DMF solvent in the MAI solution can help to enhance the reaction between PbI$_2$ and MAI, improve the MAPbI$_3$ crystallinity and grain size, and improve the device
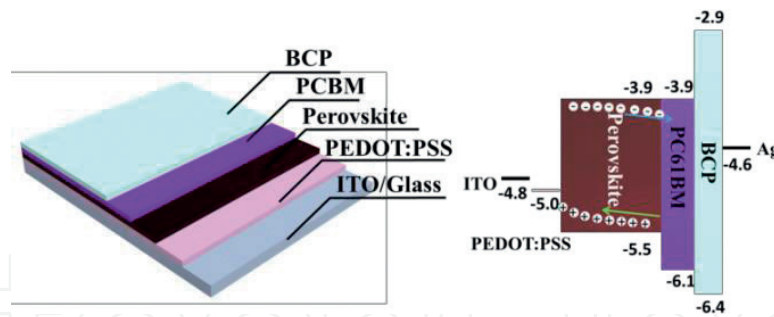
Figure 11. Device architecture of the perovskite solar cell (glass/ITO/PEDOT:PSS/perovskite/PC61BM/BCP/Ag) and the corresponding energy level diagram of corresponding materials used in the device (reprinted with the permission from [31], 2017, the Royal Society of Chemistry).
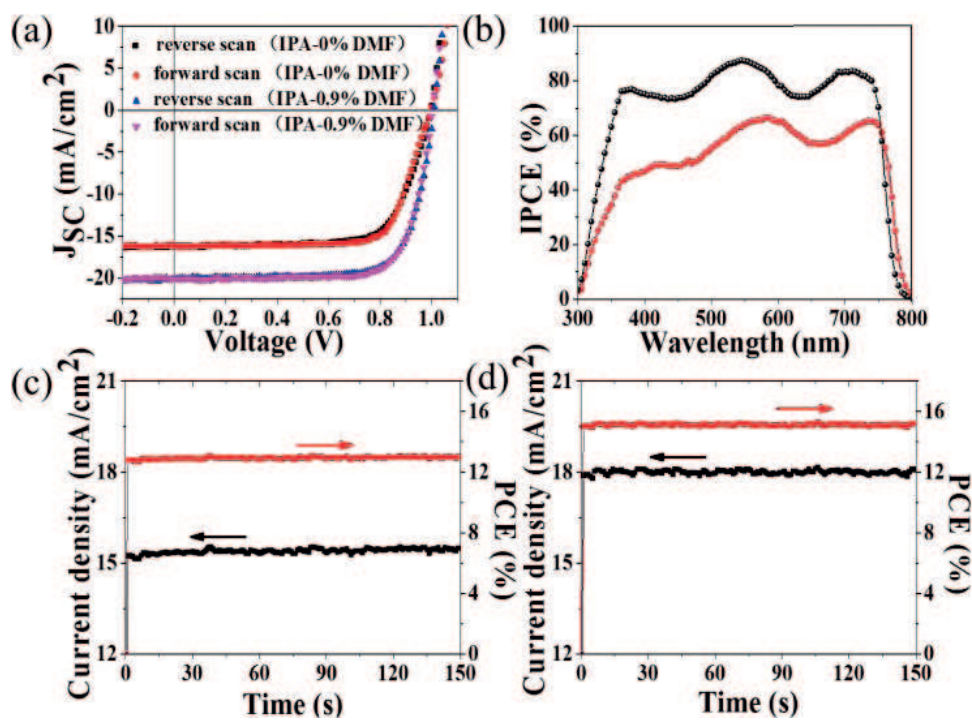

Figure 12. (a) *J–V* curves with different scanning directions at the condition of IPA and IPA- 0.9%DMF. Reverse (1.1 V → -0.2 V) and forward scan (−0.2 V → 1.1 V) measurement: the voltage step is 0.01 V. (b) IPCEs for the PSCs from MAI/IPA (red curves) and MAI/(IPA- 0.9%DMF)(black curves). Steady-state current density and PCE of the devices without (c) and with (d) DMF additive in MAI solution (Reprinted with the permission from [31], 2017, The Royal Society of Chemistry).

performance. The incident photo-to-electron conversion efficiency (IPCE) curves of the PSCs with/without DMF additive are shown in **Figure 12(b)**. The device with DMF additive shows a higher IPCE value than the device without the DMF additive, which is same as the improved efficiency of the device with DMF additive obtained from the *J–V* curve measurement.

As the photocurrent hysteresis behavior is a common issue in accurate characterization of device efficiency, the photocurrent hysteresis behaviors of PSCs with/without DMF additive were measured by changing the scanning directions (reverse scan (from a positive bias 1.1 V to a negative bias −0.2 V) and forward scan (from a negative bias −0.2 V to a positive

bias 1.1 V)). **Figure 12(a)** displays the J–V characteristics of PSCs under different scan directions. Regardless of scan directions, highly consistent J–V curves and negligible photocurrent hysteresis are observed. This indicates the validity of our measured device performance. To further verify that the measured efficiency is reliable, we also measured steady-state outputs of current density and PCE. The measurements are set at the maximum power point for the steady-state PCE and J outputs. As shown in **Figure 12(c)**, the device without DMF additive also shows a stable current density, yielding a stabilized PCE of 11.4%. Meanwhile, the device with DMF additive also shows a stable current density, yielding a stabilized PCE of over 15% as shown in **Figure 12(d)**. This result further verifies the validity of our measured device performance.

Figure 13 displays the statistic results of the fabricated PSCs. Those statistic parameters clearly reveal that the DMF additive in the MAI solution could significantly enhance the photovoltaic performance of PSCs. It should be noted that the statistic results were based on 20 perovskite solar cell devices in several batches, which indicates that our experiments are reproducible. It confirms the validity of above discussion. Surprisingly, a champion device with a PCE of 19.2% is obtained during the optimization. The corresponding device exhibited the $JSC = 23.4$ mA/cm², $VOC = 1.03$ V, and $FF = 79.6\%$, while a $JSC = 16.3$ mA/cm², $VOC = 1.01$ V, and $FF = 74.7\%$ belong to the champion cell without DMF, as displayed in **Figure 14**. At the same time, it should be noted that although the above discussion is on the device with DMF additive, devices with the GBL additive has the same trend, which shows that the method is a general method to enhance the PSC performance.
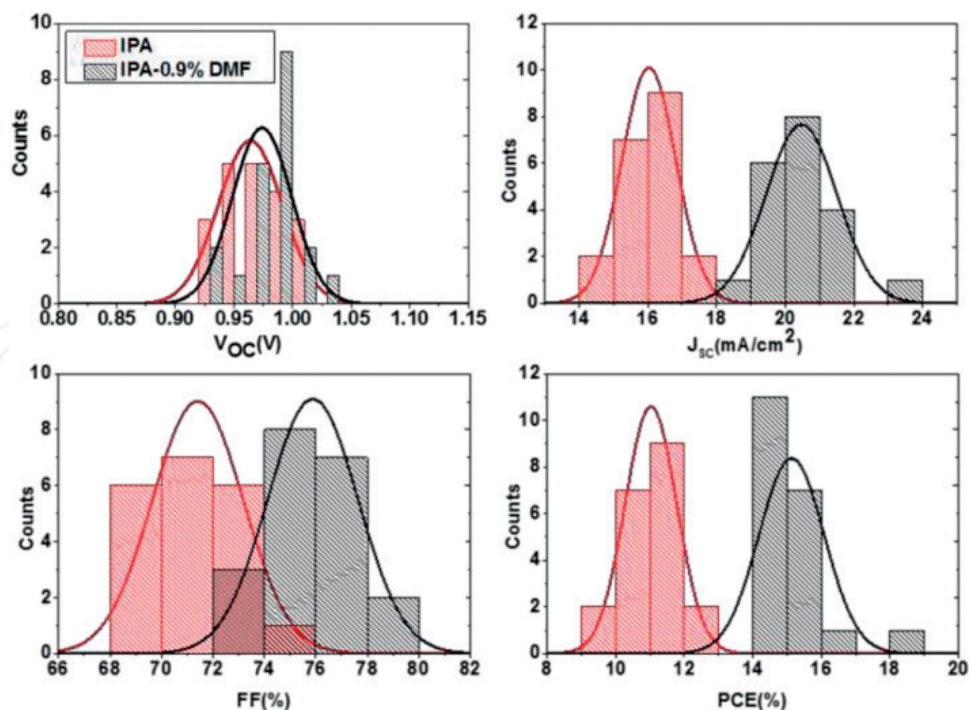

Figure 13. Comparison of histograms of photovoltaic parameters for the perovskite solar cells based on MAI/IPA (red) and MAI/(IPA-0.9%DMF) (black) condition. Data from 20 cells were used for the histogram (reprinted with the permission from [31], 2017, the Royal Society of Chemistry).
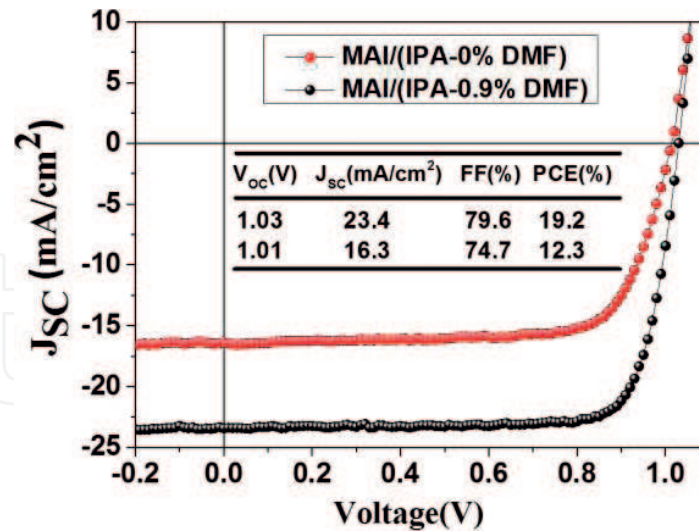
Figure 14. *J–V* curves for the best device (with or without 0.9%DMF) under standard AM1.5 simulated illumination (reprinted with the permission from [31], 2017, the Royal Society of Chemistry).

4. Conclusions

Organolead halide perovskites are emerging photovoltaic materials for next-generation solar cells. To obtain high-performance PSCs with good stability, the perovskite film with improved crystallinity, homogeneity, and surface morphology is of great importance. This chapter introduces the solvent treatment mechanisms of mixed-solvent-vapor annealing and polar solvent additive in the typical one-step and two-step perovskite deposition methods. These treatments effectively improve the perovskite film quality as well as the photovoltaic performance of planar PSCs with inverted structure. In details, compared to the alone IPA solvent annealing in one-step method, the introduction of a little polar aprotic solvent such as DMF is effective to improve the device performance. The XRD and SEM analysis demonstrates that the average grain size and crystallinity of perovskite film have been increased via IPA/DMF mixed solvent-vapor annealing (100:1, v/v). The PCE of the $CH_3NH_3PbIxCl_3$-x planar heterojunction solar cell increases from 14.0% of the pristine PSC to 17.3% of the IPA PSC and further to 18.0% of the IPA/DMF PSC and shows negligible $J - V$ hysteresis. In addition, the PSC stability is significantly improved treated by IPA/DMF mixed-solvent vapor. Our results show that the mixed-solvent-vapor annealing is a simple and promising method for PSCs and other photoelectric devices. For the interdiffusion of two- step sequential deposition, a small ratio of DMF solvent addicted into the MAI/IPA solution can help the complete conversion of PbI_2 into perovskite, which leads to the reduced pinholes, improved film morphology, increased grain sizes, enhanced film light absorption, and charge transport ability. The improved perovskite film quality is responsible for the enhancement of JSC and PCE for PSCs with inverted structure. Using this method, an optimized PCE as high as 19.2% was acquired for $CH_3NH_3PbIxCl_3$-x PSCs. In short, these two solvent treatment strategies could provide guidelines to further improve the perovskite quality and fabricate more efficient perovskite solar cells with good stability, which is essential to realize their commercialization in the future.

Acknowledgements

Author details

Shangzheng Pang and Dazheng Chen*

*Address all correspondence to: dzchen@xidian.edu.cn

State Key Discipline Laboratory of Wide Band Gap Semiconductor Technology, School of Microelectronics, Xidian University, Xi'an, China

References

[1] Kojima A, Teshima K, Shirai Y, Miyasaka T. Organometal halide perovskites as visible-light sensitizers for photovoltaic cells. Journal of the American Chemical Society. 2009;**131**: 6050-6051. DOI: 10.1021/ja809598r

[2] Dong Q, Fang Y, Shao Y, Mulligan P, Qiu J, Cao L, Huang J. Electron-hole diffusion lengths > 175 μm in solution-grown CH3NH3PbI3 single crystals. Science. 2015;**347**:967-970. DOI: 10.1126/science.aaa5760

[3] Shi D, Adinolfi V, Comin R, Yuan M, Alarousu E, Buin A, Chen Y, Hoogland S, Rothenberger A, Katsiev K, Losovyj Y, Zhang X, Dowben P a, Mohammed OF, Sargent EH, Bakr OM. Low trap-state density and long carrier diffusion in organolead trihalide perovskite single crystals. Science (80-.). 2015;**347**:519-522. DOI: 10.1126/science.aaa2725

[4] Stranks SD, Eperon GE, Grancini G, Menelaou C, Alcocer MJP, Leijtens T, Herz LM, Petrozza A, Snaith HJ. Science. 2013;**342**:341-344

[5] Xing G, Mathews N, Sun S, Lim SS, Lam YM, Grätzel M, Mhaisalkar S, Sum TC. Electron-hole diffusion lengths exceeding 1 micrometer in an organometal trihalide perovskite absorber. Science (80-.). 2013;**342**:344-347. DOI: 10.1126/science.1243982

[6] Chang J, Zhu H, Li B, Isikgor F, Hao Y, Xu Q, Ouyang J. Boosting the performance of planar heterojunction perovskite solar cell by controlling the precursor purity of perovskite materials. Journal of Materials Chemistry A. 2016;**4**:887-893. DOI: 10.1039/c5ta08398b

[7] Jeon NJ, Noh JH, Yang WS, Kim YC, Ryu S, Seo J, Il Seok S. Compositional engineering of perovskite materials for high-performance solar cells. Nature. 2015;**517**:476. DOI: 10.1038/nature14133

[8]   Yang WS, Noh JH, Jeon NJ, Kim YC, Ryu S, Seo J, Il Seok S. High-performance photovoltaic perovskite layers fabricated through intramolecular exchange. Science. 2015; **348**:1234. DOI: 10.1126/science.aaa9272

[9]   Zhang W, Eperon GE, Snaith HJ. Metal halide perovskites for energy applications. Nature Energy. 2016;**1**:16048. DOI: 10.1038/NENERGY.2016.48

[10]   Eames C, Frost JM, Barnes PRF, O'Regan BC, Walsh A, Islam MS. Ionic transport in hybrid lead iodide perovskite solar cells. Nature Communications. 2015;**6**:7497. DOI: 10.1038/ncomms8497

[11]   Brivio F, Walker AB, Walsh A. Atomistic origins of high-performance in hybrid halide Perovskite solar cells J. Appl. Maternité. 2013;**1**, 042111. DOI: 10.1021/nl500390f

[12]   Yin W, Shi T, Yan Y. Unique properties of halide perovskites as possible origins of the superior solar cell performance. Advanced Materials. 2014;**26**:4653. DOI: 10.1002/adma.201306281

[13]   Yin WJ, Yang JH, Kang J, Yan Y, Wei SH. Halide perovskite materials for solar cells: A theoretical review. Journal of Materials Chemistry A. 2015;**3**:8926. DOI: 10.1039/c4ta05033a

[14]   Chang J, Lin Z, Zhu H, Isikgor F, Xu QH, Zhang C, Hao Y, Ouyang J. Enhancing the photovoltaic performance of planar heterojunction perovskite solar cells by doping the perovskite layer with alkali metal ions. Journal of Materials Chemistry. A. 2016;**4**:16546.b. DOI: 10.1039/c6ta06851k

[15]   Heo JH, Han HJ, Kim D, Ahnb TK, Im SH. Hysteresis-less inverted $CH_3NH_3PbI_3$ planar perovskite hybrid solar cells with 18.1% power conversion efficiency. Energy & Environmental Science. 2015;**8**:1602. DOI: 10.1039/c5ee00120j

[16]   Wu CG, Chiang CH, Tseng ZL, Nazeeruddin MK, Hagfeldt A, Grätzel M. High efficiency stable inverted perovskite solar cells without current hysteresis. Energy & Environmental Science. 2015;**8**:2725. DOI: 10.1039/c5ee00645g

[17]   Gang L et al. Pressure-induced Bandgap optimization in lead-based Perovskites with prolonged carrier lifetime and ambient Retainability. Advanced Functional Materials. 2017;**27**(3). DOI: 10.1002/adfm.201604208

[18]   Ye Y et al. Top and bottom surfaces limit carrier lifetime in lead iodide perovskite films. Nature Energy. 2017): 16207;**2**. DOI: 10.1038/nenergy.2016.207

[19]   Tianran C et al. Origin of long lifetime of band-edge charge carriers in organic– Inorganic lead iodide perovskites. Proceedings of the National Academy of Sciences. 2017:04421. DOI: 10.1021/acs.jpclett.5b01361

[20]   Yang WS, Park BW, Jung EH, et al. Iodide management in formamidinium-lead- halide–based perovskite layers for efficient solar cells. Science. 2017;**356**(6345):1376-1379. DOI: 10.1126/science.aan2301

[21]   Kim BS, Choi MH, Choi MS, Kim JJ. Composition-controlled organometal halide perovskite via CH 3 NH 3 I pressure in a vacuum co-deposition process. Journal of Materials Chemistry A. 2016;**4**:5663. DOI: 10.1039/C6TA00168H

[22] Bi C, Shao Y, Yuan Y, Xiao Z, Wang C, Gao Y, Huang J. Understanding the formation and evolution of interdiffusion grown organolead halide perovskite thin films by thermal annealing. Journal of Materials Chemistry A. 2014;**2**, 18508. DOI: 10.1039/C4TA04007D

[23] Park SM, Noh YJ, Jin SH, Na SI. Efficient planar heterojunction perovskite solar cells fabricated via roller-coating. Solar Energy Materials & Solar Cells. 2016;**155**:14. DOI: 10.1016/j.solmat.2016.04.059

[24] Sun X, Zhang C, Chang J, Yang H, Xi H, Lu G, Chen D, Lin Z, Lu X, Zhang J, Hao Y. Mixed-solvent-vapor annealing of perovskite for photovoltaic device efficiency enhancement. Nano Energy. 2016;**28**:417. DOI: 10.1016/j.nanoen.2016.08.055

[25] Eperon GE, Burlakov VM, Docampo P, Goriely A, Snaith HJ. Morphological control for high performance, solution-processed planar heterojunction perovskite solar cells. Advanced Functional Materials. 2014;**24**:151-157. DOI: 10.1002/adfm.201302090

[26] Yu Y et al. Ultrasmooth Perovskite film via mixed anti-solvent strategy with improved efficiency. ACS Applied Materials & Interfaces. 2017;**9**(4):3667-3676. DOI: 10.1021/acsami.6b14270

[27] Jeng JY, Chiang YF, Lee MH, Peng SR, Guo TF, Chen P, Wen TC. $CH_3NH_3PbI_3$ Perovskite/fullerene planar-heterojunction hybrid solar cells. Advanced Materials. 2013;**25**:3727-3732. DOI: 10.1002/adma.201301327

[28] Leijtens T, Eperon GE, Noel NK, Habisreutinger SN, Petrozza A, Snaith HJ. Stability of metal halide perovskite solar cells. Advanced Energy Materials. 2015;**5**. DOI: 10.1002/aenm.201500963

[29] Sun K, Chang J, Isikgor FH, Li P, Ouyang J. Efficiency enhancement of planar perovskite solar cells by adding zwitterion/LiF double interlayers for electron collection. Nanoscale. 2015;**7**:896-900. DOI: 10.1039/C4NR05975A

[30] Shao Y, Xiao Z, Bi C, Yuan Y, Huang J. Non-wetting surface-driven high-aspect-ratio crystalline grain growth for efficient hybrid perovskite solar cells. Nature Communications. 2015;**5**:5784-5784. DOI: 10.1038/ncomms8747

[31] Mo J, Zhang C, Chang J, Yang H, Xi H, Chen D, Lin Z, Lu G, Zhang J, Hao Y. Enhance planar perovskite solar cells efficiency via two-step deposition by using DMF as additive to optimize crystal growth behavior. Journal of Materials Chemistry A. 2017;**5**:13032-13038. DOI: 10.1039/C7TA01517H